LA-UR-16-29026
Approved for public release; distribution is unlimited.

Title: Effect of Pressure Gradients on the Initiation of PBX-9502 via Irregular (Mach) Reflection of Low Pressure Curved Shock Waves

Author(s): Hull, Lawrence Mark
Miller, Phillip Isaac
Moro, Erik Allan

Intended for: This report will be included in the LANL FY16 NSR&D Year-End Report to NA-12.

Issued: 2016-11-28

Effect of Pressure Gradients on the Initiation of PBX-9502 via Irregular (Mach) Reflection of Low Pressure Curved Shock Waves

Lawrence M. Hull, Phillip I. Miller, and Erik A. Moro

Introduction

In the instance of multiple fragment impact on cased explosive, isolated curved shocks are generated in the explosive. These curved shocks propagate and may interact and form irregular or Mach reflections along the interaction loci, thereby producing a single shock that may be sufficient to initiate PBX-9501. However, the incident shocks are divergent and their intensity generally decreases as they expand, and the regions behind the Mach stem interaction loci are generally unsupported and allow release waves to rapidly affect the flow. The effects of release waves and divergent shocks may be considered theoretically through a "Shock Change Equation".

2D Shock Change Equation

A form of the energy equation for reactive flow can be developed, using a model with the chemistry of reaction lumped into a reaction rate and the equation of state, that describes the response and stability of the flow, called the Shock Change Equation by Fickett and Davis[1]. This approach follows the development in Fickett and Davis, but increases the dimensionality. The 3-dimensional equations of reactive flow are

$$\dot{\rho} + \rho\vec{\nabla}\cdot\vec{V} = 0$$

$$\dot{\vec{V}} + v\vec{\nabla}p = 0$$

$$\dot{E} + p\dot{v} = 0$$

$$\dot{\vec{\lambda}} = \vec{r}$$

Complex treatment of the chemistry is accomplished by treating λ as a vector in reaction space, and inclusion of the mechanical coupling such as hot spot collapse is captured through the EOS. Here, we consider the simplest situation, λ is a single scalar parameter and we treat the energy equation and reaction rate by introducing the equation of state

$$E = E(p, v, \lambda)$$

$$dE = E_p dp + E_v dv + E_\lambda d\lambda$$

$$\dot{p} = c^2\dot{\rho} + \rho c^2 \sigma r \qquad 1$$

with the frozen sound speed

$$c^2 = v^2(p + E_v)/E_p$$

and the definition

$$\rho c^2 \sigma = -E_\lambda / E_p$$

Now expand the vector equations in two dimensions with velocities u and w in the x-direction and y-direction respectively

$$\dot{\rho} + \rho\left(u_x + w_y\right) = 0 \qquad 2$$

$$u_t + uu_x + wu_y + vp_x = 0 \qquad 3$$

$$w_t + uw_x + ww_y + vp_y = 0 \qquad 4$$

and eliminate $\dot{\rho}$ from Eq. 1

$$\dot{p} + \rho c^2\left(u_x + w_y\right) = \rho c^2 \sigma r \qquad 1a$$

We are interested in how the pressure may change as we follow an arbitrary point in space, conveniently on the shock structure (e. g. the Mach stem). Such a point is assumed to move qausi-steadily at velocity D in the x-direction and velocity w_T in the y-direction. Mathematically, we are simply following an arbitrary point, of assumed velocity, in a two-dimensional flow. Here, we will continue to use Cartesian coordinates, but for the interested reader, Molder[2] has recently developed curved shock relations (without chemical reaction) in normal and tangential (to the shock) coordinates. Additionally, Hornung[3], using Cartesian coordinates, has studied pressure gradients in curved shock reactive flow. From the total differential of the pressure following the point

$$(dP)_T = p_t dt + p_x dx + p_y dy$$

we get

$$\left(\frac{dp}{dt}\right)_T = p_t + Dp_x + w_T p_y \qquad 5$$

Similarly

$$\left(\frac{du}{dt}\right)_T = u_t + Du_x + w_T u_y \qquad 6$$

and

$$\left(\frac{dw}{dt}\right)_T = w_t + Dw_x + w_T w_y \qquad 7$$

Now, add Eq. 5 to Eq. 1a and simplify

$$\left(\frac{dp}{dt}\right)_T + (u-D)p_x + (w-w_T)p_y + \rho c^2\left(u_x + w_y\right) = \rho c^2 \sigma r \qquad 8$$

add Eq. 6 to Eq. 3 and simplify

$$\left(\frac{du}{dt}\right)_T + (u-D)u_x + (w-w_T)u_y + vp_x = 0 \qquad 9$$

add Eq. 7 to Eq. 4

$$\left(\frac{dw}{dt}\right)_T + (u-D)w_x + (w-w_T)w_y + vp_y = 0 \qquad 10$$

The pressure on the shock is related to the particle velocity (particularly on the Hugoniot) by

$$\left(\frac{dp}{dt}\right)_T = \left(\frac{dp}{du}\right)_H \left(\frac{du}{dt}\right)_T \qquad 11$$

Similarly, one expects feature growth rates (e. g. Mach stems) to increase with the pressure, although the relationship includes the geometry of the interaction as well as the equation of state. One might consider a reaction zone with a finite transverse or lateral extent. Increasing the pressure will increase the reaction rate at this transverse boundary causing a tendency for the lateral extent of the reaction zone to increase (the reaction tries to turn the corner). So, we may heuristically take

$$\left(\frac{dp}{dt}\right)_T = \left(\frac{dp}{dw}\right)_T \left(\frac{dw}{dt}\right)_T \qquad 12$$

Eliminating $\left(\frac{du}{dt}\right)_T$, $\left(\frac{dw}{dt}\right)_T$, u_x, w_y from Eqs. 8-12, and setting u_y and $w_x = 0$ (for inviscid irrotational flow so that shear/vorticity terms are assumed negligible) because we are interested in a flow in which shock wave effects dominate the equations of motion, results in

$$\left(\frac{dp}{dt}\right)_T = \frac{-p_x\left[\frac{c^2-(D-u)^2}{D-u}\right] + p_y\left[\frac{c^2-(w-w_T)^2}{w-w_T}\right] + \rho c^2 \sigma r}{1 + \rho c^2\left[\frac{\left(\frac{du}{dp}\right)_H}{(D-u)} - \frac{\left(\frac{dw}{dp}\right)_T}{(w-w_T)}\right]} \qquad 13$$

or

$$\left(\frac{dp}{dt}\right)_T = \frac{\rho c^2\left[\sigma r - \frac{\eta p_x}{\rho(D-u)} - \frac{\beta p_y}{\rho(w_T-w)}\right]}{1+\rho(D-u)(1-\eta)^{-1}\left(\frac{du}{dp}\right)_H + \rho(w_T-w)(1-\beta)^{-1}\left(\frac{dw}{dp}\right)_T} \qquad 14$$

Where η and β are the sonic parameters

$$\eta = 1 - \frac{(D-u)^2}{c^2}$$
$$\beta = 1 - \frac{(w_T-w)^2}{c^2}$$

Some authors replace the flux terms, $\rho(D-u)$ with $\rho_0 D$ in a 1D analysis, using the shock jump continuity equation. In consideration of our application, that of chemical reaction in a 2D Mach reflection, the velocities are discontinuous in magnitude at the triple point, because of the contact discontinuity (slip line) that begins there. However, the boundary condition along the slip line is that the pressures are equal on either side and that the flow direction is the same on either side. This is similar to the boundary condition used in inviscid irrotational flow along a solid boundary in that slip is allowed but the normal velocities match (typically zero through a solid boundary). Note that the inclusions of dissipative effects such as viscosity or thermal diffusion remove the velocity discontinuity. Define the flow direction along the contact discontinuity (positive total turning angle) as

$$\tan\delta = \frac{w-w_T}{u-D} = \frac{w_T-w}{D-u}$$

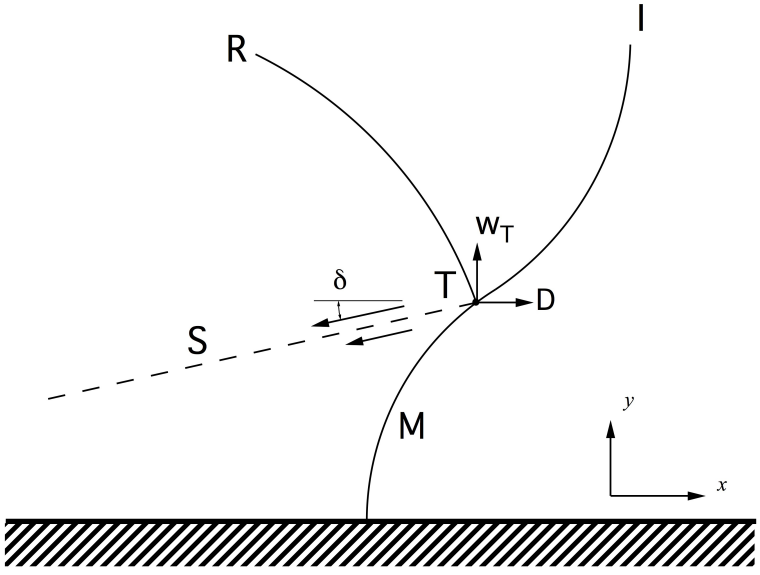

Fig. 1. Symmetric reflection of curved incident shocks, I, develop curved Mach stems and reflected shocks, M, and R, as well as a contact discontinuity (slip stream) S.

(refer to Fig. 1) and introduce into Eq. 14 to get

$$\left(\frac{dp}{dt}\right)_T = \frac{\rho c^2 \left[\sigma r - \frac{\eta p_x}{\rho(D-u)} - \frac{\beta p_y}{\rho(D-u)\tan\delta}\right]}{1 + \rho(D-u)\left[(1-\eta)^{-1}\left(\frac{du}{dp}\right)_H + \tan\delta\,(1-\beta)^{-1}\left(\frac{dw}{dp}\right)_T\right]} \qquad 15$$

It is easily seen by inspection that Eq. 15 reduces to that given in Ref. 1 in the one-dimensional case.

The thus derived 2D Shock Change Equation, Eq. 15, provides insight into the interplay between the energy released by chemical reaction and the convection into or away from a reacting region caused by pressure gradients. The Mach stem shock configuration under consideration, Fig. 1, shows that $\tan\delta$ is positive and that $\rho(D-u)$ is positive and therefore, the influence of the pressure gradients on the sign of the numerator may be investigated to determine if the flow is steady, dying, or accelerating. It is also interesting to note that the longitudinal velocity D does not have to be the CJ detonation velocity in order for steady conditions to exist, and sub- and super-detonative behavior is included.

The energy added to the flow by reaction is represented by σr. The usual Taylor wave behind a reaction zone, and our coordinates, are such that $p_x > 0$ and the mass flux through the shock is positive, so the longitudinal pressure gradient is seen to advect energy away from the reaction zone, and if large enough, will lead to failure of the reaction. The transverse pressure gradient is most often negative (higher pressure near the plane of symmetry or a wall). In situations where there is a release wave on a transverse free surface of the explosive (e. g. a failure wedge experiment), $p_y < 0$ and in this case, $\tan\delta < 0$ because the gas expands away from the plane of symmetry. Equation 15 successfully describes failure wedge behavior: When the lateral convection, the term involving p_y, overcomes the energy addition σr, the reaction may also fail. Menikoff[4] mentions this "competition with burn rate" in his assessment of barrier experiments, which are rate sticks with embedded inert materials that perturb, destabilize, and sometimes quench the detonation.

In a symmetric Mach reflection, incident shock waves collide and when the shock interaction angle is favorable, the Mach stem forms. Such a wave structure amplifies the pressure, and can initiate reaction in an explosive in this region with modest amplitude incident shocks (too small to cause reaction, $r \cong 0$) and the single shock of the stem avoids the shock desensitization effect. The shock change equation, Eq. 15, provides insight to this situation as well. At the triple point the conditions of interest are, $p_y < 0$ and $\tan\delta > 0$. So the effect of the transverse pressure gradient term is opposite to that in a failure wedge, and tends to provide pressure amplification in the Mach stem and consequently supports the initiation of reaction and subsequent flow acceleration. The longitudinal pressure gradient will be positive, if a release wave is following the structure as in the classical Taylor wave. Once again, if this gradient becomes too steep, the reaction will extinguish.

Oscillatory and galloping detonations have been observed, particularly in gas phase detonation. Such effects have been traced to the effects of transverse waves[5].

In application to the PBX-9502 Mach stem initiation experiments, we observe Mach stems that are both curved and are growing. Reactive flow, under certain circumstances, allows simultaneous adjustment of the reaction rate, the flow deflection, and the shock curvature. Thus, when the shocks are curved, there is no requirement for the Mach stem to grow. Further, if the reaction causes the Mach stem to invert curvature, it is then possible that the transverse pressure gradient will begin to detract from the reaction and tend to draw energy away from the reaction zone because the gas can expand away from the center line (as in a wedge or rate stick).

We now turn to a brief discussion of reaction rate models and their calibration data. Classically, Pop plot data is captured by driving a plane shock into a wedge with an explosive plane wave lens, covered with an attenuator that controls the incident shock pressure, and measuring the run to detonation[6]. Such a situation creates a flow where $p_y \cong 0$ because of the large width of the plane wave driver shock and $p_x \cong 0$ over the reaction zone length because of the large thickness of explosive behind the sample. Equation 15 suggests that, under this loading, if started ($\sigma > 0$), the reaction will build to detonation. Flyer plate impact experiments also usually produce sustained (flat topped) shocks, so that $p_x = 0$ for an extended duration. However, a few PBX-9502 initiation studies exist in which the flat top width is intentionally varied, called short shock flyer plate impact experiments[7,8,9]. After overtake of the shock by the rarefaction, p_x has always been seen to have an effect, and in multiple fragment impact, one expects that there will be no flat top shocks anywhere. Initiation by single fragment impact has classically considered the effect of release waves starting from the edges of the fragment or from the rear surface of the fragment. However, it is relatively difficult to effectively and independently control the pressure gradients because of difficulties with impact orientation and with unintentionally changing other variables in order to achieve control. At the same time, the recent studies on barriers create somewhat complex shock conditions that include the effects of pressure gradients and flow divergence, and have emphasized recognition that the pressure gradients are key in determining if a shock-to-detonation transition occurs[4].

Mach Reflection PBX-9502 Initiation Experiments

In order to describe fragment impact for a single fragment, many variables must be specified, and to conduct experiments, all these variables must be controlled. These variables include the impact location, the roll, yaw, and pitch for the fragment orientation at impact, along with the six associated velocities $(v_x, v_y, v_z, \dot{\theta}, \dot{\phi}, \dot{\psi})$. To these, we must add the geometry of the fragment in full detail, the material characteristics, and so on. When multiple fragments are involved, the experimental problem is duly compounded. While all of these variables will influence the details of the various shock structures developed in the explosive, all these structures will have certain overall similarities. We intend to study initiation via Mach stem formation, and we recognize that all the shocks will be similarly

curved and divergent (except possibly at the Mach stem), and all the shocks will similarly have at least two-dimensional pressure gradients attached within the reaction or partial reaction zones. There are no flat-topped shocks generated by fragment impact except in carefully contrived (and lucky) situations. Nevertheless, the triangle-like and divergent curved shocks may interact, form Mach reflections, and thereby generate conditions that could initiate PBX-9502 even when the incident shocks are too low amplitude and/or too brief in duration to initiate the explosive. Our approach in this work uses an explosive driver system to generate curved shocks that will undergo Mach reflection in a known location, and incorporate features that allow controlled variation of the pressure gradient behind the Mach stem. Access for multiple diagnostics is accomplished by using wedge geometry. Because the run-to-detonation is large for low-pressure shocks, the overall size of the wedge is fairly large.

The shot assembly is shown in Fig. 2. The driver explosive is initiated near the attenuator, and the attenuator thickness and material are varied to control the pressure, pressure gradients, and curvature of the incident shock waves. The barriers are W-Ni-Fe plates that eliminate the interaction of the detonation waves in the driver explosive, and delay their collision so that, along with the variation of the fill material between the barrier plates, the variation of the longitudinal pressure gradient behind the shock wave reflection (Taylor wave behind the Mach stem) in the PBX-9502 is effected and controllable.

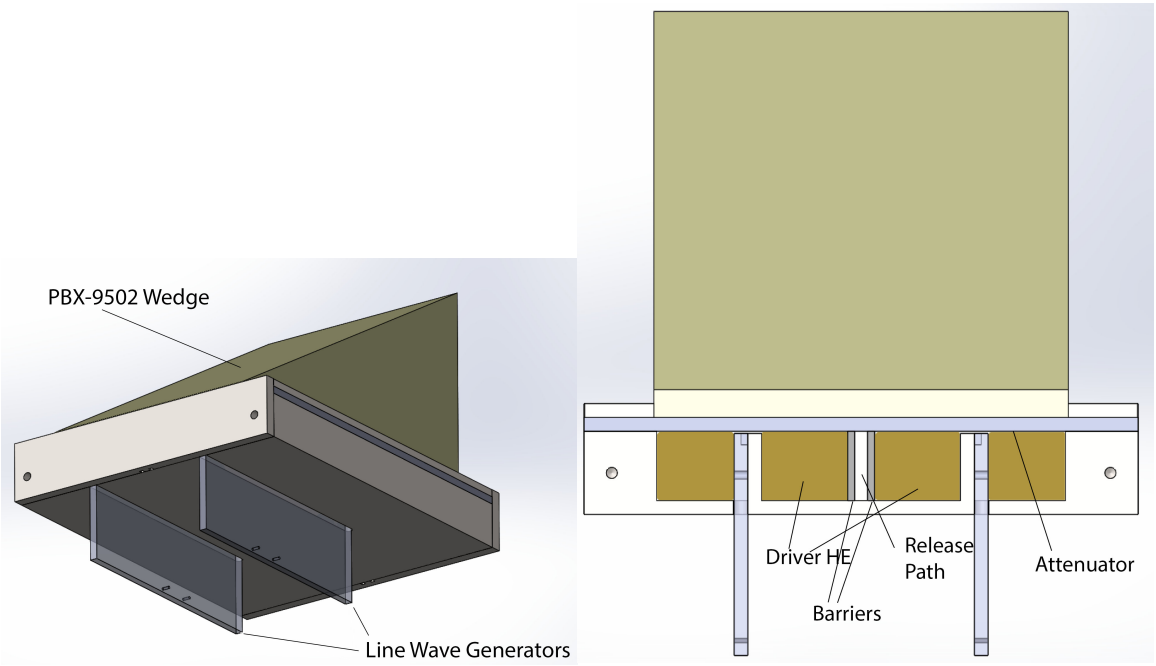

Fig. 2. Wedge and driver system

The suite of diagnostics is sketched in a view perpendicular to the slanted wedge face in Fig. 3.

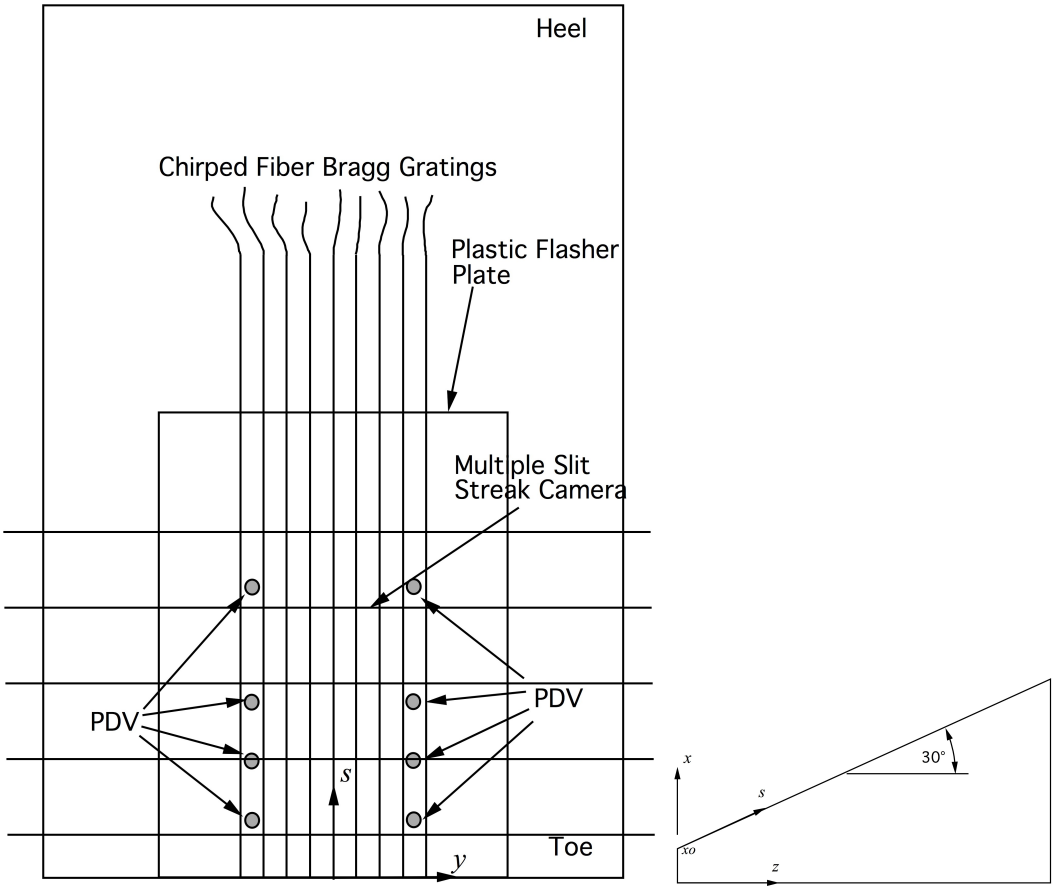

Fig. 3. A framing camera measures the shape of the shock wave using the air flash, and the streak camera measures the arrival time of the shock wave as it arrives at the slant surface. The progression of the shock wave up the slant surface is measured by the chirped fiber Bragg gratings. The PDV measures the incident shock free surface velocity, from which the incident shock pressure is estimated. An x-ray also images the barrier plates to assess their performance. Shot coordinates are also defined.

H4938

The driver consists of two line wave generators that initiate a layer of Detasheet explosive. The attenuator is a ¼" layer of aluminum (6061 T-6) that separates the Detasheet from the 9502 and the driver initiation lines are 1.5 mm below the attenuator, but very near the Detasheet-aluminum interface. The line wave generators themselves are mounted on ¼" plastic flanges to prevent pre-initiation of the Detasheet they are embedded in.

The wedge was populated with 9 chirped fiber Bragg gratings, 8 PDV probes, a framing camera and a streak camera. An x-ray was used to image the driver system. The cover plate shown was elevated 0.030" above the slanted explosive face with orange shim stock to act as a flasher for the streak and framing cameras, to tamp the chirped fiber Bragg fibers, and to hold the PDV probes in place. The PDV probes were arranged to provide only a 3 mm working distance and were intended to capture the incident shock intensity or the shock intensity of the Mach stem once

the stem has grown enough. All diagnostics reported data. The shot is seen on the shot table ready to fire in Fig. 4.

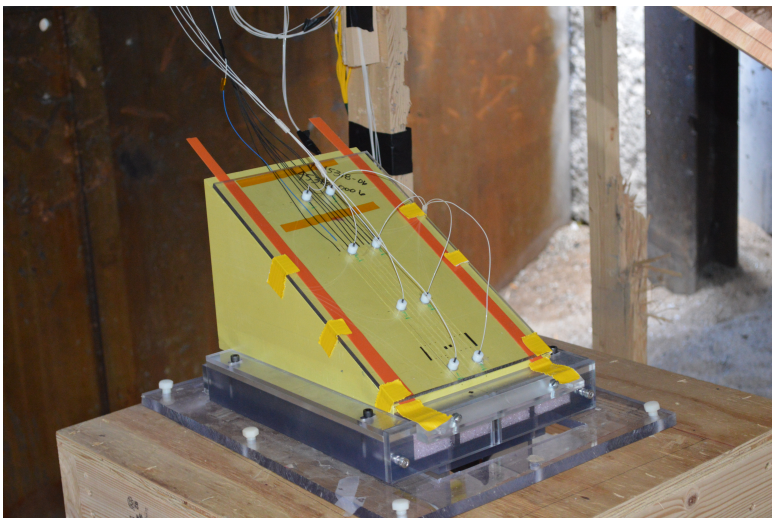

Fig. 4 The wedge was arranged with the camera views perpendicular to the angled surface of the wedge.

The framing camera data is presented as an overlay with the static in Fig. 5. The curved incident shocks and the Mach stems can clearly be seen. The timing of the images and the spatial progress of the Mach stem indicate sub-detonation velocities at this point in the experiment. Extrapolated run-to-detonation data (Pop Plot) suggest the run will be over 100 mm in the normal direction through the charge.

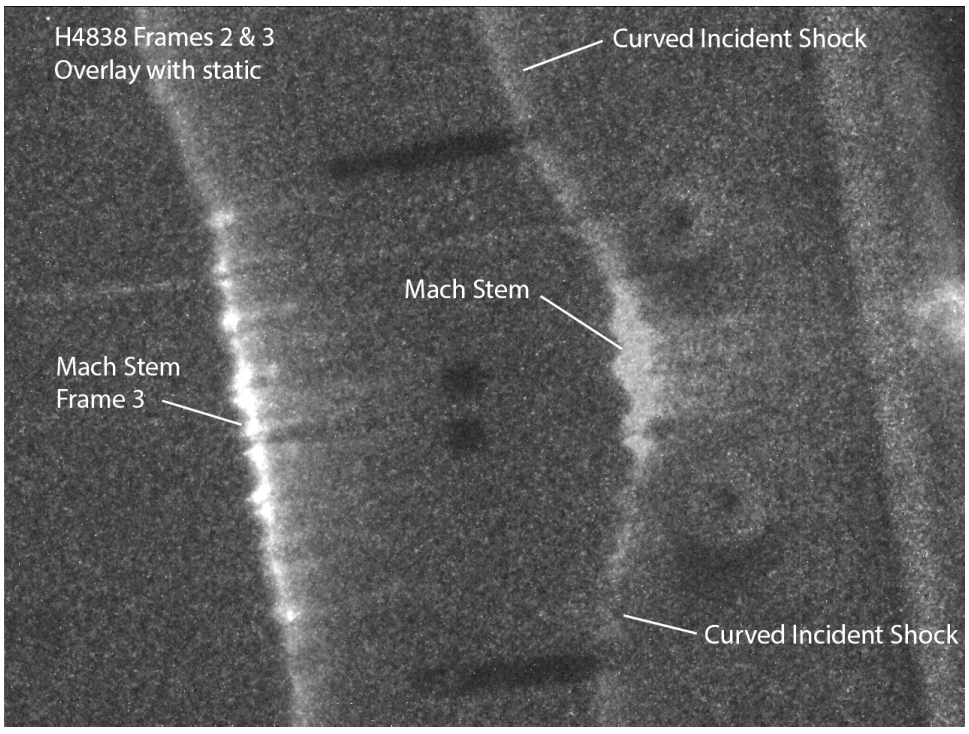

Fig. 5. Two framing camera images of the incident shocks and Mach Stems are superimposed with the static framing camera image.

The streak camera was arranged with 5 slits at a position on the charge corresponding to a perpendicular run of 35 mm, as measured from the bottom surface of the charge to the angled surface at the center slit. This corresponds to $s = 44.6$ mm. The latest time slit was not over the active area of the photocathode and did not report. The resolution could also be much better (these are problems to be corrected by the camera manufacturer). Nevertheless, the arrival time traces can still be extracted from the image, Fig. 6, to quantify the velocity and size of the Mach stem, Fig. 7 and 8.

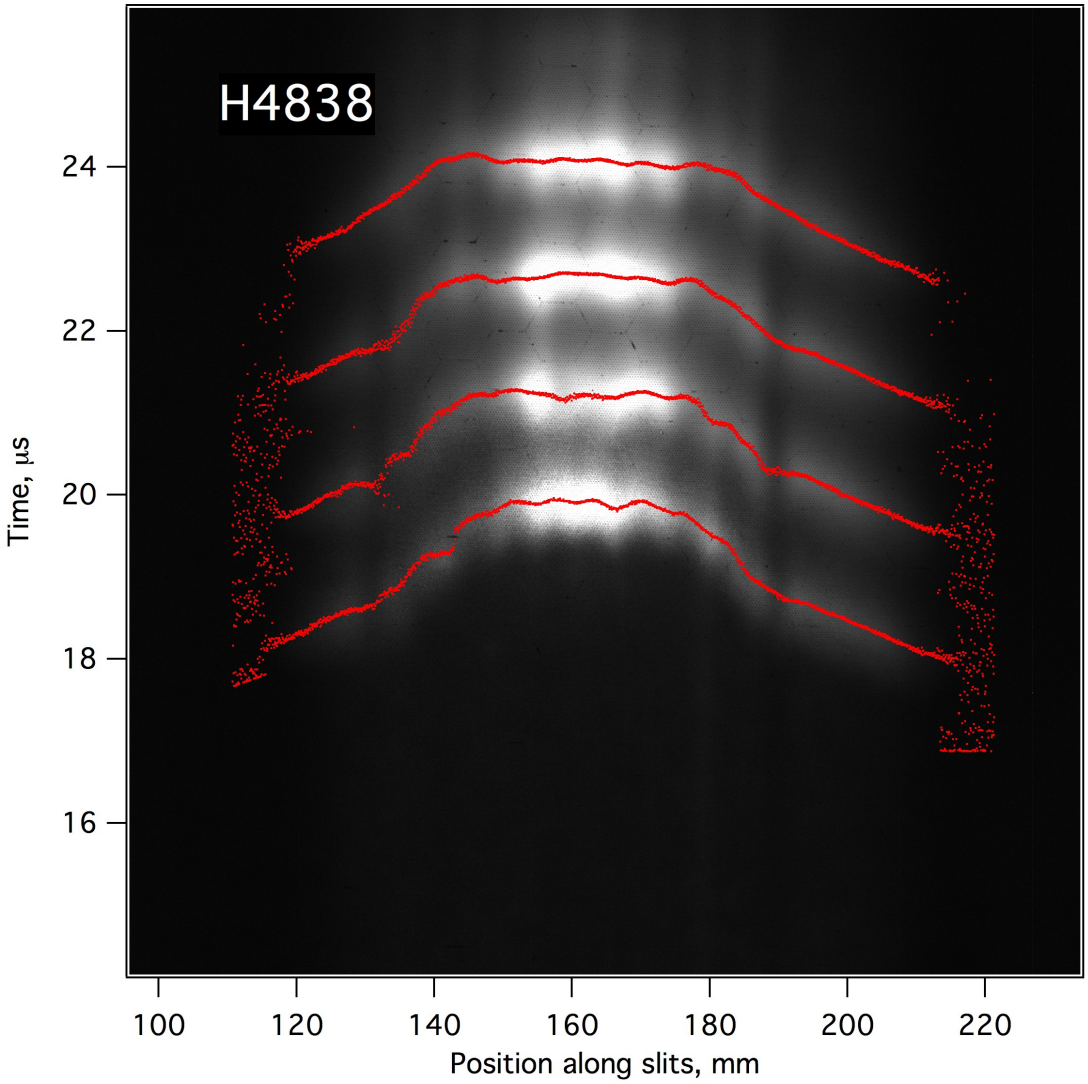

Fig. 6. Image data from the Optronis streak camera with the extracted arrival time traces superimposed.

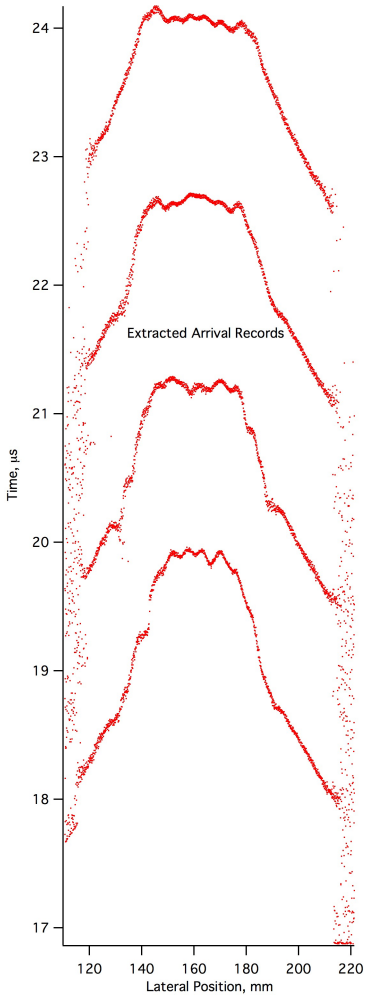

Fig. 7. Arrival times.

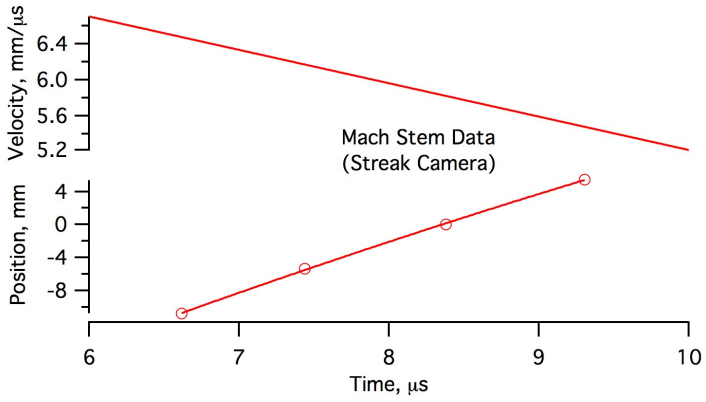

Fig. 8 Derived Mach stem velocity data from the streak camera.

The velocity shown in Fig. 8 is the phase velocity of the shock along the angled surface of the wedge. Therefore, the shock velocity will be half of the (30° wedge) values shown. These values are sub-detonative, starting at 27 kbar and decreasing slightly with distance. The Mach stem widths from Fig. 7 are 20 mm, 31 mm, 34 mm, and 40 mm. These are all well above the failure thickness of the 9502.

The PDV free surface velocity data are shown in Fig. 9. The PDV gauges were located as given in the following table. The "a" value is the lateral distance from the center of the charge (also the center of the Mach stem). The "s" distance is along the 30° face of the wedge, and the distance "h" is the run distance of the shock measured from the bottom surface of the wedge ($h = \frac{1}{2}s + 12.7\ mm$). The probes were placed with a 88.9 mm spacing along the 30° face.

Probe	a, mm	s, mm	h, mm
1	-15.9	17.7	21.55
2	+15.9	17.7	21.55
3	-15.9	106.6	66.0
4	+15.9	106.6	66.0
5	-15.9	195.5	110.45
6	+15.9	195.5	110.45
7	-15.9	284.4	154.9
8	+15.9	284.4	154.9

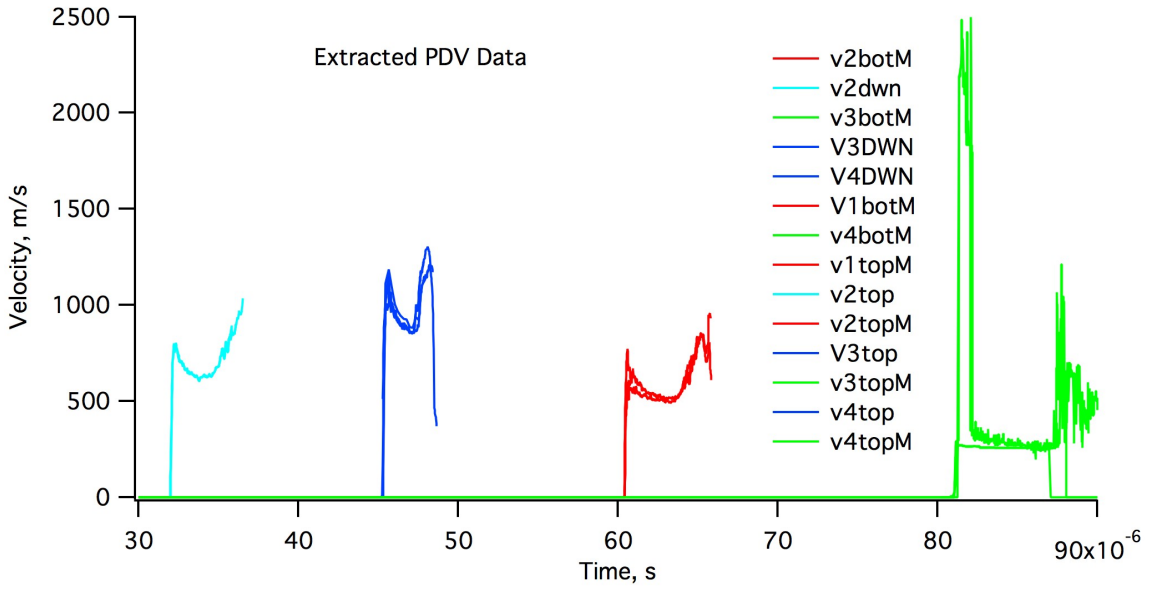

Fig. 9. Free-surface velocity as measured at 8 locations along the charge surface.

Using the known Hugoniot of the unreacted 9502 gives a pressure of about 20 kbar at the earliest probe location. At the second probe location (blue), the pressure is about 32 kbar. Note from Fig. 5 that the Mach stem is now driving the PDV probe and this probably accounts for the increase in pressure. At the third probe location (red), the velocity and therefore the pressure is degrading, and at the fourth location as well. All of the traces show signs of either some reaction or that the explosive has de-bonded into a cloud of very fine particles. This is responsible for the peak at the jump-off. On one side of the charge in the fourth location (green), the gas or particle cloud is at much higher velocity. These features indicate that there is some reaction, but it is clearly not a steady detonation.

The chirped fiber Bragg grating data is shown in Fig 10 for the probes that at least start outside the Mach stem. There are various regions of interest in this data, but the most noticeable and important attribute, for this study, is that there is no

acceleration to a steady detonation. The initial high phase velocity is due to the collision of the circular shock waves. Exactly on the centerline, this phase velocity starts out at infinity and drops quadratically. There are some bumps of acceleration around 40 and again at 45 μs. These are believed to be caused by density variations in the explosive, since the explosive was made from separate pressed pieces and was glued together at these locations.

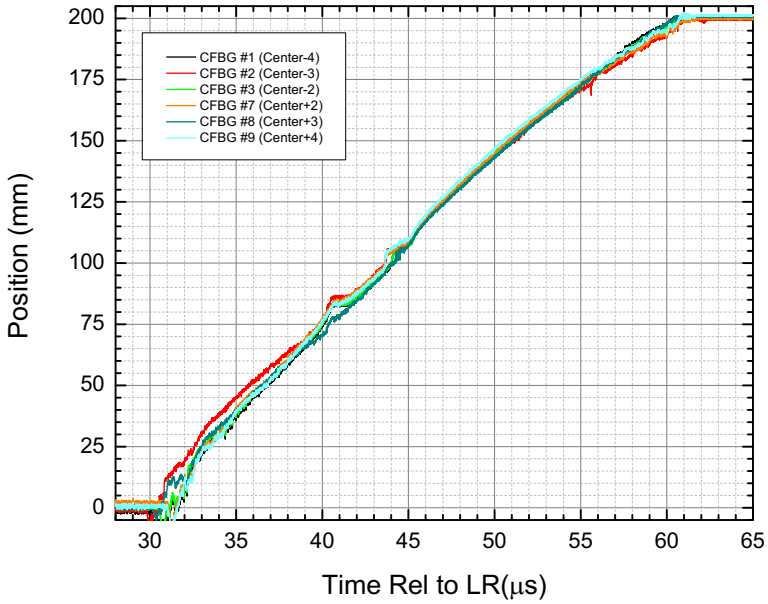

Fig. 10. Chirped fiber Bragg data initially outside the Mach stem.

The center fiber (#5) shows similar bumps and acceleration phases, Fig. 11. The surface position vs time record has been analyzed to estimate the Mach stem velocity, Fig. 11. This shows that, although the initial velocity is high, the quadratic drop quickly brings the velocity down to sub-detonative levels.

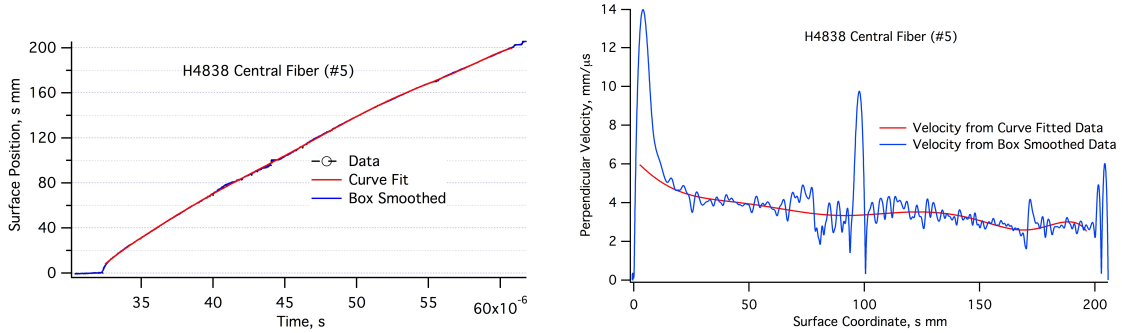

Fig. 11. Fiber 5 data and estimated velocity perpendicular to the attenuator plate.

Although the raw data is fairly dense, differentiation results in very noisy velocity estimates. The data was fit to a polynomial to obtain one velocity estimate, and was numerically smoothed to obtain the other. Note that the curve fit cannot fit the toe of the data, and also does not follow the bumps and fine features. A seen in the figure, after the drop off from the toe, the velocity settles down to a normal shock

velocity of about 4 mm/μs. This corresponds to a pressure calculated from the unreacted Hugoniot of approximately 53 kbar, and the extrapolated run-to-detonation is about 90 mm. The experiment allowed for a run of no more than 100 mm, so given some variability, it is unclear that the experiment was large enough to display a buildup to detonation. However, there seems to be no evidence of continuous acceleration, and so it is clear that $\dot{p} \leq 0$ in the shock change equation, Eq. 15. In particular, it seems apparent that in the toe region of high shock velocity, even up to twice the CJ velocity, reaction was not sustained and is likely to have been quenched by the competition with p_x. Although the width of the single shock Mach stem structure might also be blamed for the lack of transition (due to shock desensitization by the incident shocks), the framing camera data shows that the Mach stem was already around twice the failure width of PBX-9502 by the time the wave reached the first PDV probe at $s = 17$mm. Thus, during at least the latter part of the super-detonative shock velocity region, the Mach stem must have been on the order of the failure thickness and larger. This further suggests that the longitudinal pressure gradient must have been the more pronounced effect that prevented transition.

H4839

Although we believe that the failure to transition to detonation in H4838 was caused by bleeding of energy out of the reaction zone through the longitudinal pressure gradient, particularly in the toe region, the Mach stem that propagated over most of the available run was too weak to be expected to transition. In H4839, we decided to increase the incident shock pressure, which also results in higher Mach stem pressure, in order to place the Mach stem expected run-to-detonation in the middle of the available run rather than right at the end where end release effects complicate the interpretation of the data. The assembly was identical to that shown in Figs. 2, 3 and 4 with the exception that the Detasheet was replaced with Composition C-4. The additional energy of the C-4 increases the incident shock pressure, but was hand-packed and therefore raises question of the uniformity of the drive. The diagnostics were all the same, with some changes in the placement intended to accommodate the shorter expected run to detonation.

An overlay of the framing camera dynamic (flash gap) data with the static is shown in Fig. 12.

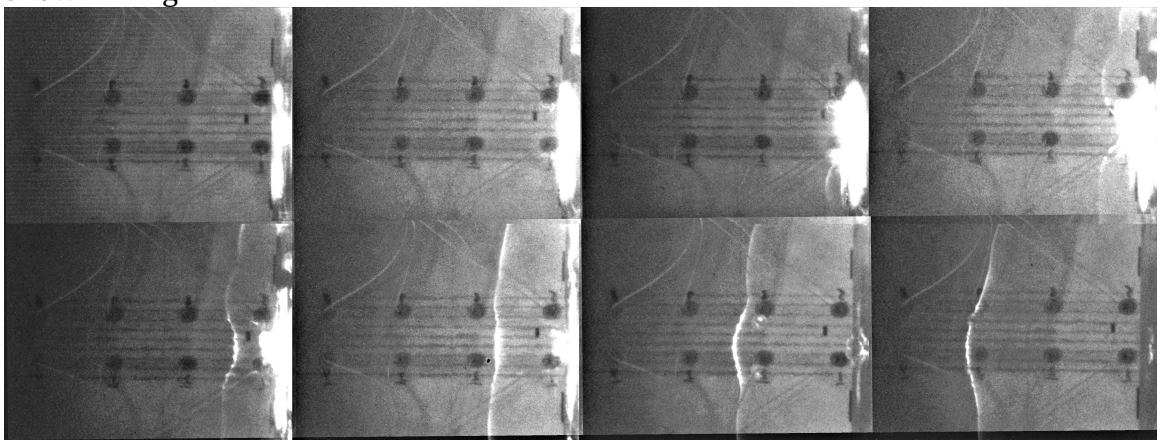

Fig. 12. H4839 static and dynamic overlay. The shock wave is just emerging from the HE products flash at the toe of the wedge in the third frame from the left, top row.

The fourth frame from the left, top row, shows the Mach stem just emerging from the products flash at the toe. It is possible to see the Mach stem in frame 4 by working with the contrast in the dynamic image, Fig. 13, and the evolution is of the stem curvature is seen in the dynamic overlay.

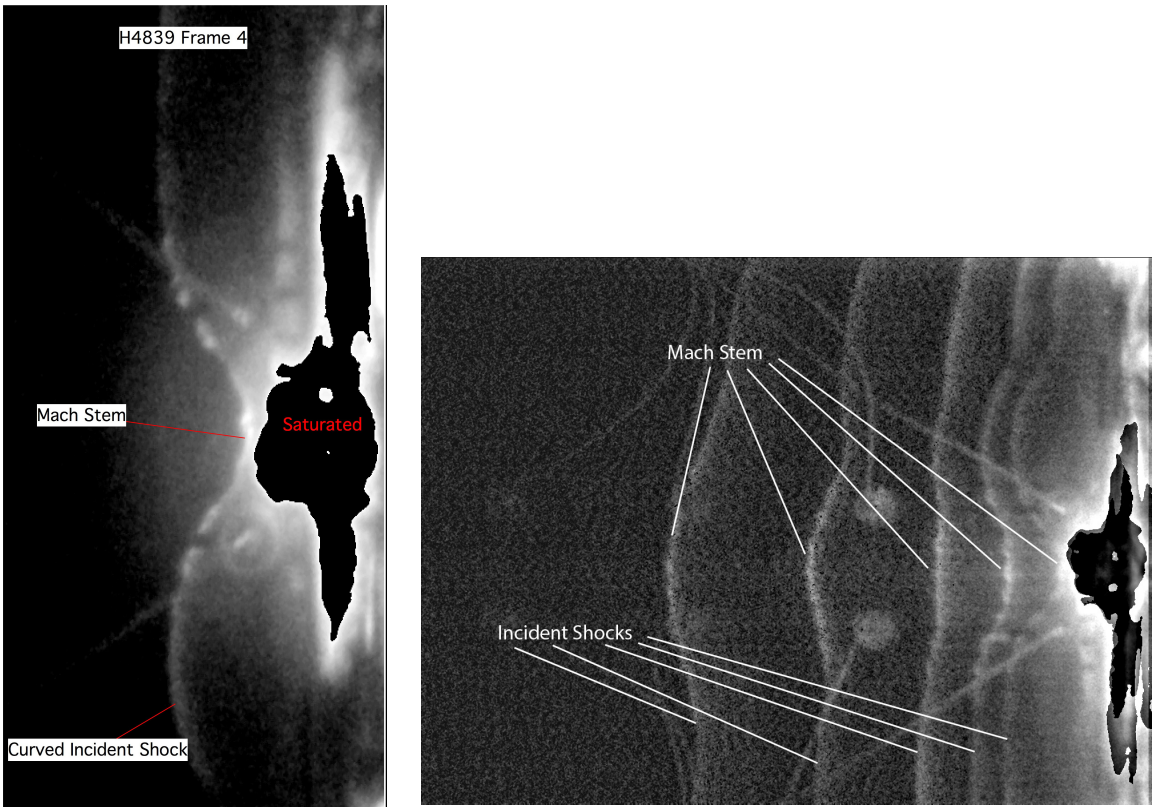

Fig. 13. Frame 4 dynamic image and compilation of dynamic 4 thru 8.

In frames 4 and 5, the Mach stem is clearly convergent. However, in frame 6 it is nearly flat, and in frames 7 and 8, the Mach stem has accelerated past the incident shock waves. This acceleration is a clear sign of reaction and suggests the flow will transition to a detonation. The Mach stem position (centerline) is

Frame	Time, μs	s, mm	y, mm
4	32.53	12.2	18.8
5	33.76	26.6	26.0
6	36	46.3	35.8
7	40	77.9	51.6
8	45	114.1	69.7

The streak camera data was located somewhat closer to the toe of the wedge in H4839, relative to H4838. The static with the slits superimposed is shown in Fig. 14 along with the dynamic.

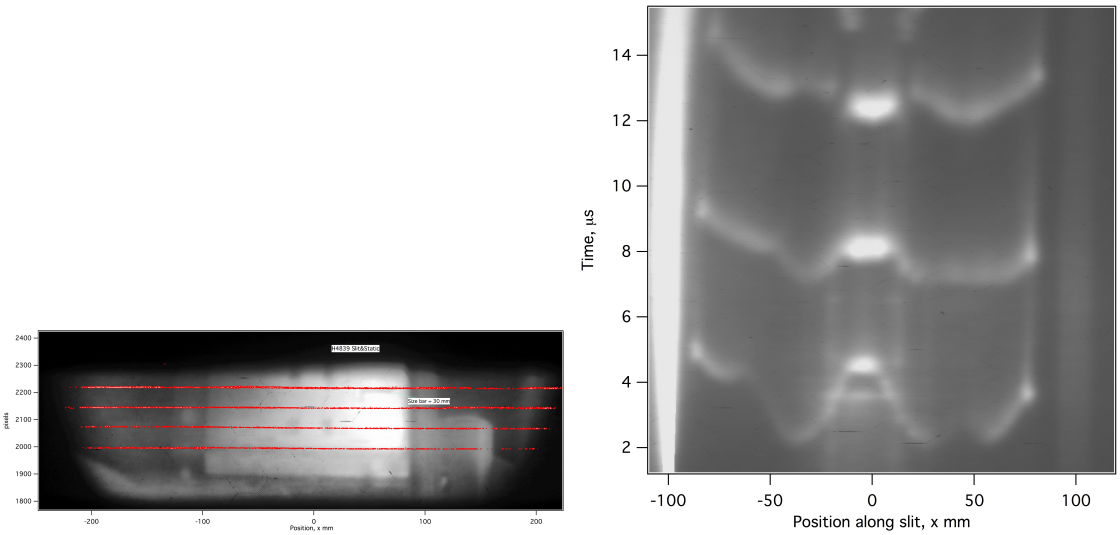

Fig. 14. Streak camera static and dynamic. Zero time is arbitrary.

The streak camera captures a wider field of view than the framing camera, and the technique measures the arrival time of the shock wave along the slits rather than directly measuring the shape. The generally, the incident shocks are captured as is the Mach stem. At the earliest time (bottom trace) the Mach stem is significantly later relative to the incident shocks. At the latest time (top trace), the Mach stem is now possibly ahead or at least coincident with the incident shocks. So, we were able to capture the acceleration of the Mach stem and the inversion of the shape in the arrival time data. The widths of the Mach stem are 15, 20, and 24 mm. Thus, the concept of the failure width is supported because the acceleration and inversion of shape occurs after the Mach stem width exceeds the failure width (the failure width is near the failure radius, or about 5 mm for PBX-9502 at 20°C[10]). It is possible that when the Mach stem accelerates due to reaction, the inversion in shape causes the central region of the reaction zone to lose the support of the incident shocks (p_y term support of reaction). Considering the shock change equation, sign reversal of the p_y term in combination with the influence of the p_x term may strongly influence further acceleration, deceleration or steadiness.

The PDV data is shown in Fig. 15. The framing camera data, Fig. 13, shows that the first set of PDV probes were swept over by the incident shock wave, not the Mach stem.

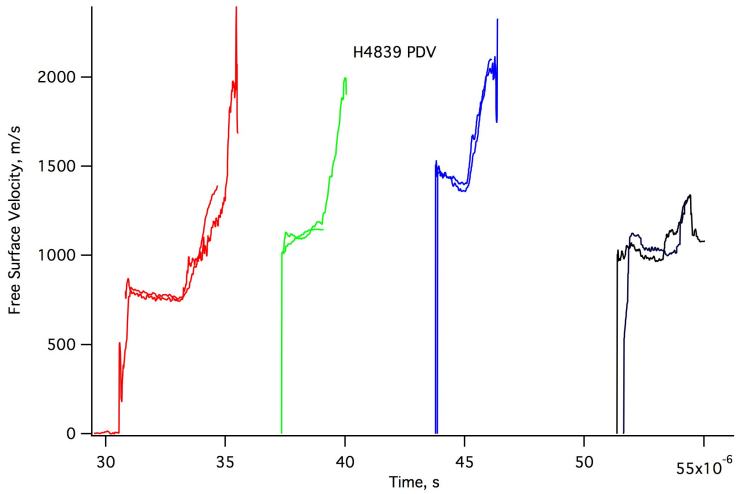

Fig. 15. H4839 PDV data.

However, the second and third set of probes was swept over by the Mach stem region during the period when the framing camera shows significant acceleration behavior, Fig. 12. By extrapolation, one might expect that the wave structure that swept over the 4th set of probes was expanded and, considering the drop in the PDV data, smoother slower wave. The first set of probes suggests that the incident shock pressure was about 25 kbar, based on the unreacted Hugoniot of PBX-9502. The third set indicates a pressure of 62 kbar, and is associated with at least a partial reaction in the Mach stem region (based on the acceleration indicated by the framing camera data). The pressure then reduces again at the fourth probe location, indicating that a full transition to detonation was not achieved.

The chirped fiber Bragg contributes information about the propagation of the incident shocks and the Mach stem. The complete data set is shown in Fig. 16.

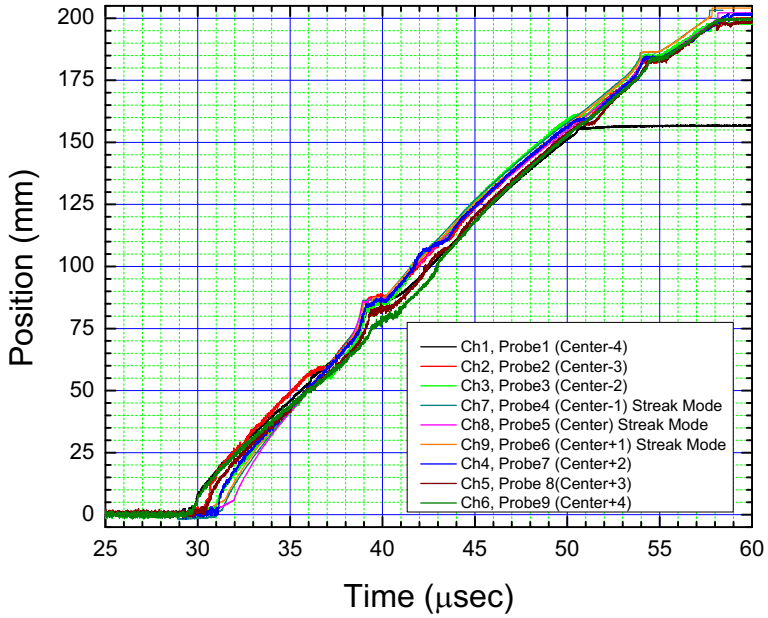

Fig. 16. The complete set of chirped fiber Bragg data for H4839.

Once again, there are bumps of acceleration and deceleration that occur at the glue joints of the part. We also generally see the initial acceleration phase followed by a gradual slowing of the wave. The same analysis technique was used to extract velocity information from the center fiber data by both smoothing and also by fitting to a polynomial, Fig. 17.

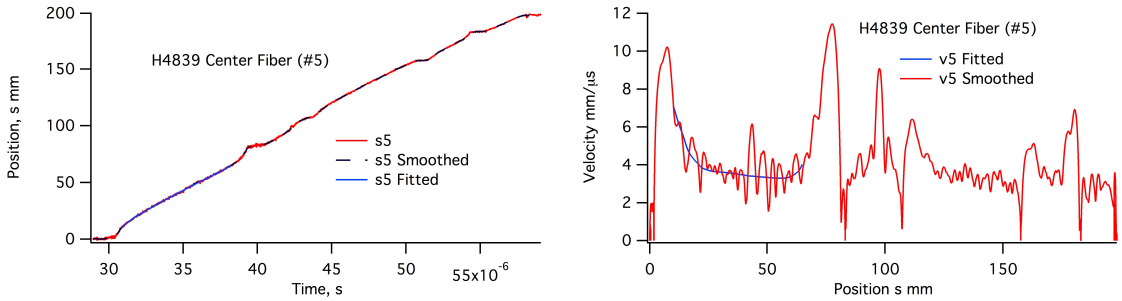

Fig. 17. Fiber 5 data and estimated velocity perpendicular to the attenuator plate.

The Mach stem velocity drops down to about 4 mm/μs, and the corresponding pressure is 53 kbar. The acceleration of the wave seen in the framing camera and streak camera occurs at s coordinate between 40 and 115 mm. This is also the region near the glue joint in the explosive parts.

Calculations

Inert calculations in 2D were done with the CTH code and Forest Fire and Surf calculations were done with the Pagosa code. Briefly, for H4839, Forest Fire did not predict transition to detonation and showed no wave acceleration, although there was a small amount of reaction on the centerline. Surf, on the other hand, predicted the wave acceleration and wave shape seen in the experiment, but also predicted that shock transitioned to a detonation running at about 7.6 mm/μs. We see that the experimental result is somewhere between the two calculations. Neither model captures the correct behavior.

The inert calculations show that a Mach stem develops and generates a pressure of about 100 kbar, and the Pop plot suggests we would transition to a detonation wave, if this were a well-supported shock. Other experiments show that Mach stems in this pressure range that are well supported (say by a detonation wave collision in the driver explosive) do indeed transition to a detonation. So, we have found an experimental design that displays a strong sensitivity to the release wave (Taylor wave) slope. This slope is adjustable in a simple way by inserting a plug in the space between the tungsten plates, Fig. 18.

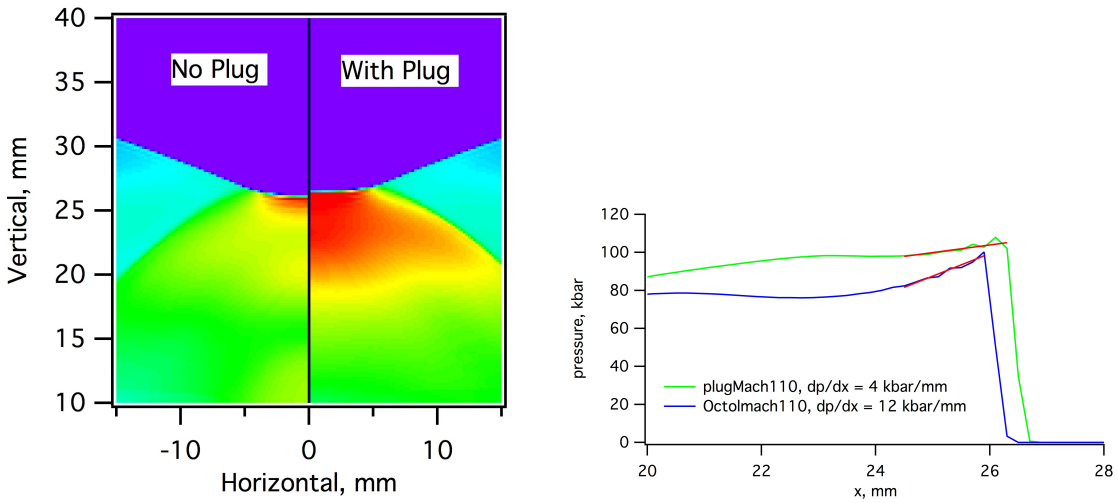

Fig. 18 CTH calculations show the effect of putting a plug in the space between the tungsten plates. The pressure plot shows red for $p \geq 100$ kbar.

Future Directions

In order to increase the incident and stem shock pressures we will move to a hotter driver explosive, Comp B is the current choice. All explosive will be machined to improve the consistency of the driver. We will run experiments with and without plugs, and the size of the plug will be varied to give various Taylor wave slopes. The glue joints will be removed from consideration by simply making the wedges from monolithic pieces of PBX-9502.

References

1) Detonation, Fickett and Davis, University of California Press, 1979 p. 101-102, p. 131-132
2) S. Molder, "Curved Shock Theory", *Shock Waves, 2015*
3) H. G Hornung, "Gradients at a curved shock in reacting flow", *Shock Waves (1998) 8: 11–21*
4) Ralph Menikoff , "Barrier experiment: Shock initiation under complex loading" December 20, 2015, Los Alamos Report LA-UR-16-20140
5) Detonation, Fickett and Davis, University of California Press, 1979, Chap. 6
6) J. J. Dick, et al, "The Hugoniot and shock sensitivity of a plastic-bonded TATB explosive PBX 9502", *J. Appl. Phys. v 63, n 10, 15 May 1988*
7) J. J. Dick, "Short Pulse Initiation of a Plastic-bonded TATB Explosive", *J. Energetic Matls., v 5, p 267, 1987*
8) C. M., Tarver, "Modeling Shock Initiation and Detonation Divergence Tests on TATB-Based Explosives", *Propellents, Explosives, Pyrotechnics I5, 132, 1990*
9) R. L. Gustavsen, S. A. Sheffield, and R. R. Alcon, "Measurements of shock initiation in the tri-amino-tri-nitro benzene based explosive PBX-9502: Wave forms from embedded gauges and comparison of four different material lots", *J. Appl. Phys, v 99, 114907, 2006*
10) A. W. Campbell, "Diameter Effect and Failure Diameter of a TATB-Based Explosive", *Propellants, Explosives, Pyrotechnics, v9, p183-187, 1984*